JOURNAL OF THE INTERNATIONAL ASSOCIATION FOR SHELL AND SPATIAL STRUCTURES: **J. IASS**

NEW IN OLD: SIMPLIFIED EQUATIONS FOR LINEAR-ELASTIC SYMMETRIC ARCHES AND INSIGHTS ON THEIR BEHAVIOR

BRANKO GLISIC

Associate Professor, Dpt. of Civil and Env. Eng., E330 EQuad, Princeton, NJ 08544, USA, bglisic@princeton.edu

Editor's Note: Manuscript submitted 06 September 2019; revision received 09 July 2020; accepted 24 August 2020. This paper is open for written discussion, which should be submitted to the IASS Secretariat no later than March 2021.

DOI: https://doi.org/10.20898/j.iass.2020.006

ABSTRACT

Closed-form equations for determination of reactions and internal forces of linear-elastic symmetric arches with constant cross-sections are derived. The derivation of the equations was initially made for segmental, three-hinged, two-hinged, and hingeless arches. Not all derived equations are simple, but still not excessively complex to apply, and they reveal several new insights into the structural behavior of arches. The first is an extremely simple approximate equation for horizontal reactions of a hingeless arch under self-weight, which could be also applied with excellent accuracy to catenary and parabolic arches, and with a desirable level of accuracy to two- and three-hinged arches with a relatively wide range of geometries. The second insight is an approximately linear relationship between reactions and between internal forces of arches with different structural systems, which helps understand the global structural behavior of arches in a new way and enables inference of some other insights presented in the paper. The third insight reflects the relationships between normal force distribution and its eccentricity in different types of arches. Finally, the fourth insight regards the comparison of behavior of arches under the self-weight with those loaded with uniformly distributed load along their span.

Keywords: *symmetric linear-elastic arch, different structural systems, horizontal reaction, closed-form equations, internal forces, self-weight, segmental (circular) shape, parabolic & catenary shapes*

1. INTRODUCTION

Mastering segmental (circular-shaped, round) arches in antiquity enabled the creation of large-scale infrastructure and the built environment through centuries. The arch as a structural system was discovered and applied in Sumerian civilization on a small scale, while the systematic use of arches started with Etruscans (e.g., [1]) in 4th century Before Common Era (BCE, also referred to as BC – Before Christ), and remained one of the main structural systems for the following two-and-one-half millennia. The most frequent shape of an ancient large-scale arch was semi-circular, but exceptions were noticed as early as in 2nd century BCE (e.g., [2]). Development of engineering mechanics and various analytical techniques from the 17th to the 19th century enabled a better understanding of the internal force distributions and stress distributions within an arch [3]. Subsequently, the arch shape diversified and took other forms, different from the segmental (e.g., elliptic, catenary, parabolic, etc.), i.e., the shape was designed from case to case so that it could optimize one or several design constraints (e.g. relative to aesthetics, materials, stress, etc.).

Probably the first description of the structural behavior of arches is given by Leonardo da Vinci who has written [4] (1508?): "An arch is nothing other than a strength caused by two weaknesses; for the arch in buildings is made up of two segments of a circle, and each of these segments being in itself very weak desires to fall, and as the one withstands the downfall of the other the two weaknesses are converted into a single strength". Robert Hooke understood how the (moment-free) arch works [3] and published in 1676 the anagram describing catenary as the ideal shape for an arch subjected to self-weight [5]. There was a lot of progress over the centuries in understanding and deepening the knowledge on arches and excellent overviews can be found in [3] and [12]. Thus, there are numerous publications accumulated over time that in a complementary manner present the analysis arches from various points of view (e.g., [1], [4-11, 13-14], just to name a few). More recent literature mostly

focuses on the non-linear analysis of arches (incl. geometric and material non-linearity, e.g., [15-16]) and buckling analysis of arches (e.g., [17]). Some recent literature still deals with linear elastic arches, including equations for moment-free arches [18] and closed-form equations for funicular arches [19].

The author of this paper derived simple closed-form expressions for reactions in segmental, catenary and parabolic arches [20]. Nevertheless, to the best of author's knowledge, accessible literature does not present simple closed-form expressions for internal forces of symmetric linear elastic segmental arches subjected to dead-loads (self-weight of the arch, weight of the deck supported by the arch, etc.).

The mathematical analysis of linear-elastic arches based on differential equations dates back to the middle of the 19th century [12] with works of Bresse (1854) [6] and Winkler (1858) [7]. Closed solutions for these equations can ease conceptual design and preliminary analysis of arches, especially for structures built in materials with linear or quasi-linear behavior such as steel, timber, or concrete. In addition, closed solutions can augment the understanding of certain properties of linear-elastic arches that are not easy to assess by methods found in literature so far, or by numerical methods such as finite element modeling (FEM) or discrete element modeling (DEM). Note that the words "conceptual" and "preliminary" are important in the statement above, as in many cases the linear-elastic approach is not sufficient or appropriate for detailed design and analysis. For detailed design and analysis, FEM or DEM with appropriate constitutive equations and boundary conditions should be used. However, the closed-form solutions can inform detailed design and analysis by helping set the initial values for models.

Hence, the aims of this paper are (i) to present closed-form expressions for reactions and internal forces of three-hinged, two-hinged and hingeless symmetric linear-elastic segmental arches with constant cross-section subjected to uniformly distributed force along the centerline (i.e., the self-weight of the arch, see Equations 5-12) and along the span (e.g., the self-weight of the deck supported by arch, see Equations 19-23), (ii) to present simple, approximate, yet accurate expressions for the determination of horizontal reactions of the hingeless and three-hinged segmental arch under the above mentioned loads, respectively (see Equations 13 and 20), and evaluate to what extent are these expression applicable to other types of segmental arches, (iii) to evaluate in detail the accuracy of expressions in their application to catenary and parabolic arches, and understand how the difference in shape affects the accuracy, (iv) to identify relationships between reactions and between internal forces in different types of arches given that they have the same geometrical and mechanical properties (but not the same structural system, see Equations 14-16 and 24), and (v) to demonstrate applicability of closed form expressions by parametric study on eccentricity of normal force in segmental arches and by comparison of reactions of the two analyzed load scenarios.

The closed-form expressions were derived based on planar linear beam theory using equations of equilibrium for the three-hinged arch, traditional force method for the two-hinged arch, and the method of elastic center (a special case of force method) for the hingeless arch. Note that for planar beam theory to be applicable, the depth of the cross-section should be significantly smaller than both the length of the arch and the radius of the arch (i.e., the ratios depth over length and depth over radius should be both smaller than approximately 1/5 [13]). These constraints are found in most real-life cases, and thus the expressions and conclusions derived in this paper have very broad applicability.

2. OVERVIEW OF GENERAL EQUATIONS OF A SEGMENTAL ARCH

In general case, differential equations of curvilinear beams are difficult or impossible to solve in closed form as they contain the radius of curvature of the beam as a term. However, for segmental (circular) beams (arches), solution is possible as the radius of curvature is constant (see Equations 1a-c). Hence, closed-form expressions for segmental arches could be derived and analyzed first, and then expanded to parabolic and catenary arches.

Let us observe typical symmetric arches with a circular shape (represented by their centerlines), as shown in Figure 1. To simplify presentation, the main geometrical parameters, as adopted in this study, are given only in Figure 1c (hingeless arch): centerline radius R, centerline span L, centerline rise D, and angle of embrace β. To simplify the formulas, β will be substituted, where appropriate, with 2α, where α is half-angle of embrace (i.e., $\alpha=\beta/2$, or $\beta=2\alpha$). The same notation applies for Figures 1a and 1b (three- and two-hinged arch, respectively).

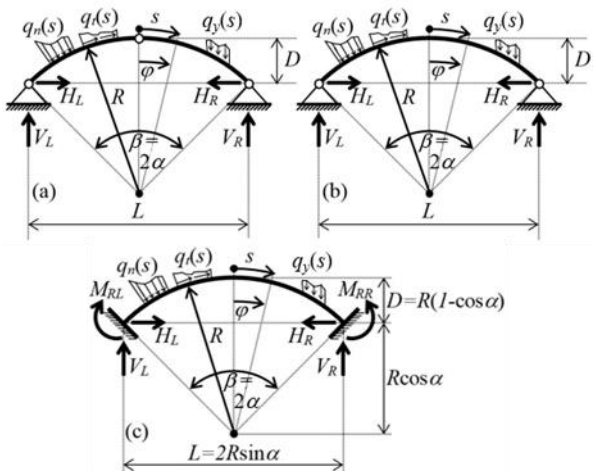

Figure 1: *a) three-hinged, b) two-hinged, and c) hingeless arch*

Let the origin of curvilinear (natural) coordinate system be taken at the apex of the arch centerline, and natural coordinate s is measured from that origin clockwise. Note that ratio s/R represents the angle φ (in radian) between the vertical line connecting the apex and the center of the circle of the arch centerline, and the line connecting point with coordinate s and the center. Let us denote vertical load with $q_y(s)$ and its normal and tangential components (to the arch centerline) with $q_n(s)$ and $q_t(s)$, respectively. Positive orientation of s, $q_y(s)$, $q_n(s)$, and $q_t(s)$ is shown in Figure 1 (this convention is chosen so that the bending moment in the arch is positive if tensioning the lower fiber of cross-section). Then, the general equations of equilibrium for the circular arch are given as follows [13]:

$$\frac{\mathrm{d}N(s)}{\mathrm{d}s} - \frac{S(s)}{R} + q_t(s) = 0 \qquad (1a)$$

$$\frac{\mathrm{d}S(s)}{\mathrm{d}s} + \frac{N(s)}{R} + q_n(s) = 0 \qquad (1b)$$

$$\frac{\mathrm{d}M(s)}{\mathrm{d}s} - S(s) = 0 \qquad (1c)$$

$$\frac{\mathrm{d}^2 S(s)}{\mathrm{d}s^2} + \frac{S(s)}{R^2} - \frac{q_t(s)}{R} + \frac{\mathrm{d}q_n(s)}{\mathrm{d}s} = 0 \qquad (2)$$

where: $N(s)$, $S(s)$, and $M(s)$ are the normal force, shear force, and bending moment, respectively;

Equations 1a-c are independent, while Equation 2 is obtained by combining Equations 1a and 1b in order to provide a solution for shear force $S(s)$ for given loads $q_n(s)$ and $q_t(s)$. To complete the solution, it is necessary to determine two constants of integration from static boundary conditions. Then, Equation 1c is used to find $M(s)$, with the third constant of integration determined from boundary conditions. Finally, $N(s)$ is determined using Equation 1b. Let us assume that only a vertical symmetric load $q_y(s)$ acts over the arch. Then, the reactions will be symmetric too and the following expressions for internal forces are valid for all three types of symmetric arches:

$$N^{q_y}(s) = -H^{q_y}\cos\frac{s}{R} - V^{q_y}\sin\frac{s}{R} + Q_y(s)\cdot\sin\frac{s}{R} \qquad (3a)$$

$$S^{q_y}(s) = H^{q_y}\sin\frac{s}{R} - V^{q_y}\cos\frac{s}{R} + Q_y(s)\cdot\cos\frac{s}{R} \qquad (3b)$$

$$M^{q_y}(s) = -H^{q_y}R\left(\cos\frac{s}{R} - \cos\alpha\right) + V^{q_y}R\left(\sin\alpha - \sin\frac{s}{R}\right) + M_R^{q_y} - M_y(s) \qquad (3c)$$

where $Q_y(s) = \int_s^{R\alpha} q_y(\xi)d\xi$ is resultant of load q_y between coordinate s and right support, $M_y(s) = \int_s^{R\alpha} q_y(\xi)R(\sin\frac{\xi}{R} - \sin\frac{s}{R})d\xi$ is the resultant moment of load q_y between coordinate s and right support (about point with coordinate s), $H^{q_y} = H_R^{q_y} = H_L^{q_y}$, $V^{q_y} = V_R^{q_y} = V_L^{q_y}$, and $M_R^{q_y} = M_{RR}^{q_y} = M_{RL}^{q_y}$ are reactions due to load q_y (see Figure 1); note that $M_R^{q_y} = 0$ for the three-hinged and two-hinged arches (no moment reactions at pin supports).

3. REACTIONS AND INTERNAL FORCES IN TYPICAL ARCHES DUE TO SELF-WEIGHT

Let us denote with $g(s)$ the self-weight of an arch distributed linearly along the centerline of the arch. Hence, at any point with coordinate s, $g(s)$ is special case of $q_y(s)$. For arch with constant cross-section made of homogeneous material $g(s)=g=constant$. The normal and tangential component of load (see Figure 1) are expressed as follows:

$$q_n(s) = g\cos\frac{s}{R};\ q_t(s) = g\sin\frac{s}{R} \qquad (4)$$

In all equations that are presented in this section, superscript g is used to denote self-weight of the arch. Self-weight g of a symmetric segmental arch will generate reactions that are symmetric with respect to the vertical axis of symmetry, i.e., $V_L^g = V_R^g = V^g$, $H_L^g = H_R^g = H^g$, and $M_{RL}^g = M_{RR}^g = M_R^g$ (see Figure 1). Due to symmetry, the vertical reaction V^g is equal to half-weight of the arch. The vertical reaction V^g, vertical force Q_y^g, and moment M_y^g (see Equations 3) are calculated as follows:

$$V_R^g = V_L^g = V^g = gR\alpha \tag{5a}$$

$$Q_y^g(s) = gR\left(\alpha - \frac{s}{R}\right) \tag{5b}$$

$$M_y^g(s) = gR^2\left(\cos\frac{s}{R} - \cos\alpha + \frac{s}{R}\sin\frac{s}{R} - \alpha\sin\frac{s}{R}\right) \tag{5c}$$

Expressions 4 and 5 are valid for all three types of arches considered in this paper, as per Figure 1. Consequently, the difference in internal forces for the three types of arches will depend only on difference in horizontal reactions H^g (exists in all three types of arches) and moment reaction M_R^g (exists only for hingeless arch), see Equations 3.

Derivation of closed-form expressions for reactions and internal forces involves approaches of classical structural analysis. In order to focus on the aims of this paper, as well as to improve its readability, these derivations, along with associated approaches are presented in part in [20] and in full detail in [21]. Only the results are presented in this section.

3.1. Reactions and internal forces in a three-hinged segmental arch loaded by self-weight

Expressions for horizontal reactions and internal forces in three-hinged segmental arch are given in Equations 6 and 7a-c, respectively. Subscript "3h" is used to emphasize that the structure is three-hinged.

$$H_{3h}^g = gR\left(\alpha\cot\frac{\alpha}{2} - 1\right) = \\ = \frac{1}{4}gL\csc\frac{\alpha}{2}\left(\alpha\csc\frac{\alpha}{2} - \sec\frac{\alpha}{2}\right) \tag{6}$$

In Equation 6, the first right-hand expression is given in terms of arch radius and half-angle of embrace, while the second is given in terms of the arch span and the half-angle of embrace. Equation 6 is simple to apply (especially the first right-hand expression) and can be directly used for conceptual design or preliminary analysis of symmetrical segmental three-hinged arches with a constant cross-section.

$$N_{3h}^g(s) = -gR\left(\left(\alpha\cot\frac{\alpha}{2} - 1\right)\cos\frac{s}{R} + \frac{s}{R}\sin\frac{s}{R}\right) \tag{7a}$$

$$S_{3h}^g(s) = gR\left(\left(\alpha\cot\frac{\alpha}{2} - 1\right)\sin\frac{s}{R} - \frac{s}{R}\cos\frac{s}{R}\right) \tag{7b}$$

$$M_{3h}^g(s) = -gR^2\left(\alpha\cot\frac{\alpha}{2}\left(\cos\frac{s}{R} - \cos\alpha\right) + \right. \\ \left. + \left(\frac{s}{R}\sin\frac{s}{R} - \alpha\sin\alpha\right)\right) \tag{7c}$$

Equations 6 and 7 are analyzed in more detail and compared to similar equations for two-hinged and hingeless arch in Subsections 3.5 and 3.6.

3.2. Reactions and internal forces in a two-hinged segmental arch loaded by self-weight

Expressions for horizontal reactions and internal forces in two-hinged segmental arch are given in Equations 8 and 9a-c, respectively. Subscript "2h" is used to emphasize that the structure is two-hinged.

$$H_{2h}^g = \frac{1}{2}gR\left(\frac{\alpha + 9\sin\alpha\cos\alpha - 10\alpha\cos^2\alpha}{\alpha - 3\sin\alpha\cos\alpha + 2\alpha\cos^2\alpha}\right. \\ \left.\frac{-4\alpha^2\sin\alpha\cos\alpha}{\alpha - 3\sin\alpha\cos\alpha + 2\alpha\cos^2\alpha}\right) \tag{8}$$

$$N_{2h}^g(s) = \\ -gR\left(\frac{\alpha + 9\sin\alpha\cos\alpha - 10\alpha\cos^2\alpha}{\alpha - 3\sin\alpha\cos\alpha + 2\alpha\cos^2\alpha}\frac{1}{2}\cos\frac{s}{R}\right. \\ \left.\frac{-4\alpha^2\sin\alpha\cos\alpha}{\alpha - 3\sin\alpha\cos\alpha + 2\alpha\cos^2\alpha}\frac{1}{2}\cos\frac{s}{R} + \frac{s}{R}\sin\frac{s}{R}\right) \tag{9a}$$

$$S_{2h}^g(s) = \\ gR\left(\frac{\alpha + 9\sin\alpha\cos\alpha - 10\alpha\cos^2\alpha}{\alpha - 3\sin\alpha\cos\alpha + 2\alpha\cos^2\alpha}\frac{1}{2}\sin\frac{s}{R}\right. \\ \left.\frac{-4\alpha^2\sin\alpha\cos\alpha}{\alpha - 3\sin\alpha\cos\alpha + 2\alpha\cos^2\alpha}\frac{1}{2}\sin\frac{s}{R} - \frac{s}{R}\cos\frac{s}{R}\right) \tag{9b}$$

$$M_{2h}^{g}(s)=-gR^{2}\cdot \left(\frac{3\alpha+3\sin\alpha\cos\alpha-6\alpha\cos^{2}\alpha}{\alpha-3\sin\alpha\cos\alpha+2\alpha\cos^{2}\alpha}\frac{1}{2}\left(\cos\frac{s}{R}-\cos\alpha\right)+\frac{-4\alpha^{2}\sin\alpha\cos\alpha}{\alpha-3\sin\alpha\cos\alpha+2\alpha\cos^{2}\alpha}\frac{1}{2}\left(\cos\frac{s}{R}-\cos\alpha\right)+\left(\frac{s}{R}\sin\frac{s}{R}-\alpha\sin\alpha\right)\right) \quad (9c)$$

Note that Equation 8, which expresses the horizontal reaction in a two-hinged arch is more complex than Equation 6, which expresses the horizontal reaction in a three-hinged arch. The appearance of the former is complex and difficult to intuitively understand. Hence, it is not practical (yet it is feasible) to use it for conceptual design or preliminary structural analysis of a two-hinged arch. Equation 8 can be simplified to a certain extent by deriving a simplified expression for the horizontal reaction of a hingeless arch and appropriately combining it with Equation 6. Equations 8 and 9 are further analyzed and compared to similar equations for the three-hinged and hingeless arch in Subsections 3.5 and 3.6.

3.3. Reactions and internal forces in a hingeless segmental arch loaded by self-weight

Expressions for horizontal reactions, internal forces, and moment reactions in hingeless segmental arch are given in Equations 10, 11a-c, and 12, respectively. Superscript "0h" is used to emphasize that the structure is hingeless (i.e., it has 0 hinges). Equation 10 is given in closed form; however, its appearance is complex and difficult to intuitively understand. Significant simplification of this equation is made in the next subsection.

$$H_{0h}^{g}=-gR\cdot\left(\frac{1}{2}+\frac{\alpha\sin^{2}\alpha+3\sin\alpha\cos\alpha-3\dfrac{\sin^{2}\alpha}{\alpha}}{\alpha+\sin\alpha\cos\alpha-2\dfrac{\sin^{2}\alpha}{\alpha}}\right) \quad (10)$$

$$N_{0h}^{g}(s)=-gR\cdot\left(-\left(\frac{1}{2}+\frac{\alpha\sin^{2}\alpha+3\sin\alpha\cos\alpha-3\dfrac{\sin^{2}\alpha}{\alpha}}{\alpha+\sin\alpha\cos\alpha-2\dfrac{\sin^{2}\alpha}{\alpha}}\right)\cos\frac{s}{R}+\frac{s}{R}\sin\frac{s}{R}\right) \quad (11a)$$

$$S_{0h}^{g}(s)=gR\cdot\left(-\left(\frac{1}{2}+\frac{\alpha\sin^{2}\alpha+3\sin\alpha\cos\alpha-3\dfrac{\sin^{2}\alpha}{\alpha}}{\alpha+\sin\alpha\cos\alpha-2\dfrac{\sin^{2}\alpha}{\alpha}}\right)\sin\frac{s}{R}-\frac{s}{R}\cos\frac{s}{R}\right) \quad (11b)$$

$$M_{0h}^{g}(s)=-gR^{2}\cdot\left(\left(\frac{3}{2}-\frac{\alpha\sin^{2}\alpha+3\sin\alpha\cos\alpha-3\dfrac{\sin^{2}\alpha}{\alpha}}{\alpha+\sin\alpha\cos\alpha-2\dfrac{\sin^{2}\alpha}{\alpha}}\right)\cdot\left(\cos\frac{s}{R}-\frac{\sin\alpha}{\alpha}\right)+\frac{s}{R}\sin\frac{s}{R}-\left(\cos\frac{s}{R}-\cos\alpha\right)\right) \quad (11c)$$

$$M_{R,0h}^{g}=-gR^{2}\cdot\left(\left(\frac{3}{2}-\frac{\alpha\sin^{2}\alpha+3\sin\alpha\cos\alpha-3\dfrac{\sin^{2}\alpha}{\alpha}}{\alpha+\sin\alpha\cos\alpha-2\dfrac{\sin^{2}\alpha}{\alpha}}\right)\cdot\left(\cos\alpha-\frac{\sin\alpha}{\alpha}\right)+\alpha\sin\alpha\right) \quad (12)$$

3.4. Simplified equation for horizontal reactions of a hingeless segmental arch loaded by self-weight

To better understand Equation 10, the dependence of the normalized horizontal reaction H_{0h}^{g} on the half-angle of embrace α (in radians) is given in Figure 2.

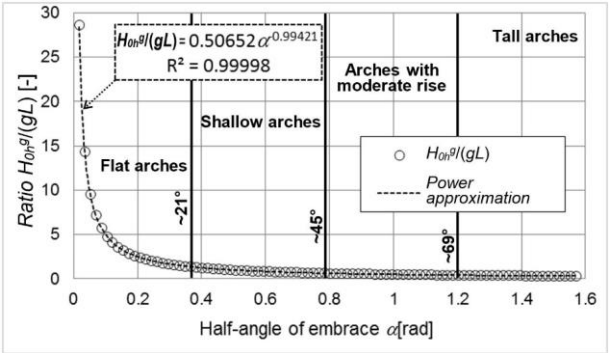

Figure 2: *Dependence of H_{0h}^{g} normalized with gL on half-angle of embrace α, and power function approximation*

Normalization is performed using product *gL*, i.e., the dependence of $H_{0h}^{g}/(gL)$ on α is presented. The

approximation of this dependence using the power function is also determined in Figure 2, based on which, the following approximate equation can be used to determine H_{0h}^{g}:

$$H_{0h}^{g} \approx \frac{gR\sin\alpha}{\alpha} = \frac{gL}{2\alpha} = \frac{gL}{\beta} \qquad (13)$$

By comparing Equations 10 and 13, it can be shown that the later underestimates the former for less than 2% (see Figure 3). In particular, the second and third right-hand terms in Equation 13 show that the horizontal reaction H_{0h}^{g} (i.e., thrust) in hingeless arch due to self-weight is approximately equal to the product of weight per unit length g and span of arch L, divided by angle of embrace $\beta=2\alpha$. Note that product gL is equal to the weight of an imaginary straight beam which bridges the same span L and has the same weight per unit length g as the arch.

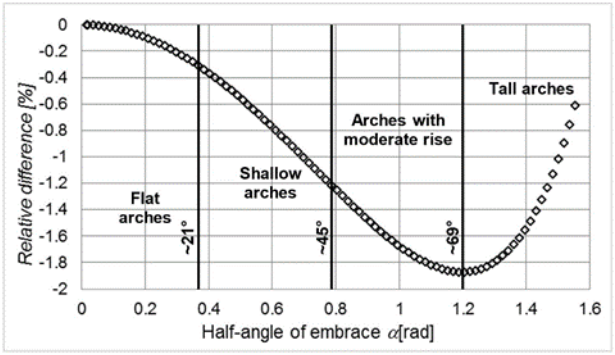

Figure 3: *Relative difference between approximate and true expression (Eq. 13 and 10, resp.) for the horizontal reaction of hingeless arch loaded with self-weight*

The approximate expression given in Equation 13 is surprisingly simple and intuitive, yet very accurate, and it can be directly used in conceptual design or preliminary analysis of hingeless segmental arches. It will be shown later in the text that this equation can be extended to three- and two-hinged segmental arches too, with some limitations in accuracy imposed by the size of half-angle of embrace α.

Figure 2 and Equation 13 show that the normalized horizontal reaction changes for relatively small values (less than 5% per degree) for half-angle of embrace equal or greater than approximately 0.37 rad (21°). For this angle the rise to span ratio D/L = 0.092 (see Figure 4) and normalized horizontal reaction $H_{0h}^{g}/(gL)$=1.368. For smaller half-angles of embrace, the rise is very small, and normalized horizontal force increases importantly as the angle decreases. These arches can be classified as "flat". Note that as the arch "flattens", the half-angle of embrace approaches to 0 rad (0°), D/L approaches to 0 (see Figure 4) and $H_{0h}^{g}/(gL)$ rises to infinity. This shows that for very small half-angles of embrace the assumptions of the linear theory might not be valid.

For half-angle of embrace equal to 1.20 rad (69°), the rise to span ratio D/L = 0.344 (see Figure 4) and the normalized horizontal reaction $H_{0h}^{g}/(gL)$=0.423. For this angle, the relative difference between Equations 13 and 10 is the largest by absolute value (-1.87%). Arches with half-angles of embrace larger than 1.20 rad (69°) can be classified as "tall". Note that for the "tallest" arch the half-angle of embrace is 1.57 rad (90°), D/L = 0.5 (see Figure 4) and $H_{0h}^{g}/(gL)$=0.320.

For half-angle of embrace of 0.79 rad (45°), the rise to span ratio D/L = 0.207 (see Figure 4) and the normalized horizontal reaction $H_{0h}^{g}/(gL)$=0.644. This value is approximately twice as low as the normalized horizontal reaction of the "least flat" arch, and approximately twice higher than the "tallest" arch. Hence, the half-angle of embrace of 0.79 rad (45°) is chosen to delimit "shallow" arches and arches with moderate rise (see Figure 4), i.e., the arches that have half-angle of embrace between 0.37 rad (21°) and 0.79 rad (45°) can be classified as shallow, and those with half-angle of embrace between 0.79 rad (45°) and 1.20 rad (69°) as arches with moderate rise (or moderate arches).

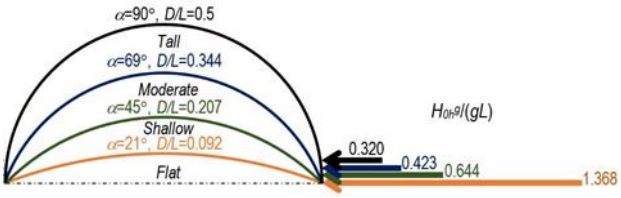

Figure 4: *Classification of arches and characteristic values of D/L, α, and $H_{0h}^{g}/(gL)$; reactions to the left are not shown to simplify the figure*

The above classification of arches eases description in further text. For illustrative purposes, Figure 4 shows the arches with the rise to span ratios that describe the above classification. Normalized horizontal reactions are shown graphically and the lengths of the arrows are drawn in proportion to the magnitude of the reactions.

3.5. Relationships between reactions and between internal forces

Expression 13 calculates the approximate value of the horizontal reaction of a hingeless arch and is both intuitive and simple to apply. Equation 6 calculates the horizontal reaction of a three-hinged arch. It is

not intuitive, but it is still simple to apply. Its graph is qualitatively similar to that shown in Figure 2, but it cannot be approximated with the power function with a sufficient degree of accuracy. Expression 8 calculates the horizontal reaction in a two-hinged arch, and while applicable, it is relatively complex and cannot be further simplified. Similar to the three-hinged arch, its graph is qualitatively similar to that shown in Figure 2, but similarly, it cannot be approximated with the power function with a sufficient degree of accuracy. A relative difference between the power-function approximation and the true equation would range from -6.4% (for flat arches) up to 19.2% (for tall arches). To explore the relationship between the horizontal reactions of the three structural systems, and to further simplify Expression 8, the horizontal reactions in the three-hinged and two-hinged arch was normalized with the horizontal reaction in a hingeless arch and graphed against the half-angle of embrace in Figure 5.

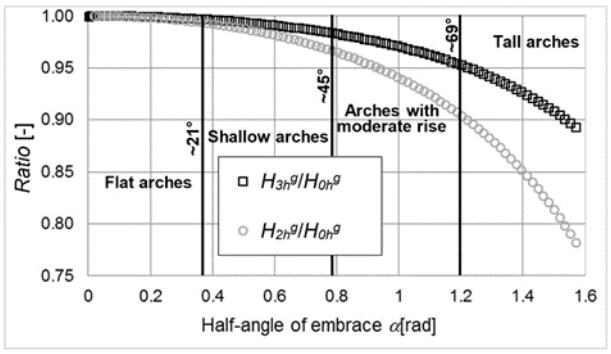

Figure 5: *Ratios between horizontal forces of the three-hinged and hingeless arch, and two-hinged and hingeless arch, as functions of half-angle of embrace*

The figure leads to several important conclusions:

(1) Figure 5 shows that the horizontal reaction is the highest for a hingeless structure and the lowest for a two-hinged structure, which is somewhat counter-intuitive in two aspects – first, one would intuitively expect the largest reaction for a determinate structure (three-hinged arch) and the lowest for the most indeterminate structure (hingeless); second, one would intuitively expect that the horizontal reaction "follows" the trend of determinacy, i.e., one would expect that the second to highest is in the two-hinged and not in the three-hinged arch; these "paradoxes" can be qualitatively explained by the facts that the two-hinged arch has the most balanced bending moment distribution, i.e., maximum and minimum are similar by absolute value, and thus the smallest horizontal reaction, while the hingeless arch has to comply with extra boundary conditions at its extremities (no rotation of cross-section) and thus the largest horizontal reaction;

(2) The applicability of Equations 6 and 13 can be understood by analyzing in more detail the relationships between the graphs shown in Figure 5; the figure shows that for flat arches there is no significant difference in the horizontal reaction between the three types of arches – the ratio for the three-hinged arches ranges between 0.997 and 1 (i.e., max. relative difference is 0.3%), while for the two-hinged arches it ranges between 0.993 and 1 (i.e., max. relative difference is 0.7%); the difference is also small for shallow arches – for the three-hinged arches the ratio ranges between 0.983 and 0.997 (max. relative difference is ranged between 0.3% and 1.7%), while for the two-hinged arches the ratio ranges between 0.966 and 0.993 (max. relative difference is ranged between 0.7% and 3.4%); in addition, the relative difference is acceptably small even for some arches with moderate rise – for the three-hinged arches the ratio ranges between 0.952 and 0.983 (max. relative difference is ranged between 1.7% and 4.8%), while for the two-hinged arches the ratio ranges between 0.903 and 0.966 (max. relative difference is ranged between 3.4% and 9.7%); finally, the difference is acceptably small for some tall three-hinged arches as the ratio ranges between 0.892 and 0.952 (max. relative difference is ranged between 4.8% and 11.8%); the above discussion leads to the following conclusions:

a. The applicability of Equation 13 can be extended to three- and two-hinged flat and shallow arches with reasonably good accuracy (as per above discussion), to some extent to three- and two-hinged arches with moderate rise (especially given that the Equation 13 underestimates the true value of Equation 12, i.e., to small extent compensate the relative difference shown in Figure 5), and even to tall three-hinged arches (depending on desired accuracy);

b. A discussion similar to one presented above can be derived for Equation 6, i.e., Equation 6 can be extended to two-hinged and hingeless flat and shallow arches, with reasonably good accuracy, and to some extent to two-hinged and hingeless arches with moderate rise and even tall arches; the main difference from point a. above is that for each half-angle of embrace Equation 6 underestimates the value of the horizontal reaction of the hingeless arch and overestimates it

for the two-hinged value for approximately the same percentage; for example, for the half-angle of embrace of 69° Equation 6 underestimates the value of the horizontal reaction in a hingeless arch for approximately 5% and overestimates the value of the horizontal reaction in a two-hinged arch for approximately the same value, i.e., 5% (see Point 3 below for more detail);

These discoveries represent an important contribution of this paper, as they broaden the applicability of Equations 13 and 6, the former being simpler and more intuitive, but providing less accurate results for the two-hinged arches with moderate rise (and tall arches), and the latter being more complex and less intuitive, but providing with approximately equally accurate results when extended to both two-hinged and hingeless arches.

(3) Probably the most unexpected conclusion from Figure 5 is that the horizontal reaction in the three-hinged arch is approximately equal to the average value of the horizontal reactions in the hingeless and two-hinged arch, i.e., the following equation applies:

$$H_{3h}^{g} \approx \frac{1}{2}\left(H_{0h}^{g} + H_{2h}^{g}\right) \tag{14}$$

If Equations 6, 8, and 10 are used in Equation 14, then the biggest absolute relative difference of -0.2% is obtained for the half-angle of embrace equal to 90°; if the simplified Equation 13 is used instead of Equation 10, then the biggest absolute relative difference of -1.0% is obtained when the half-angle of embrace ranges between 62° and 79°;

An important consequence of Equation 14 is that the normal and shear forces obey to the same relationship, while bending moment follows a slightly modified relationship, as shown in Equations 15a-c (see also Equations 3a-c);

$$N_{3h}^{g}(s) \approx \frac{1}{2}\left(N_{0h}^{g}(s) + N_{2h}^{g}(s)\right) \tag{15a}$$

$$S_{3h}^{g}(s) \approx \frac{1}{2}\left(S_{0h}^{g}(s) + S_{2h}^{g}(s)\right) \tag{15b}$$

$$\begin{aligned} M_{3h}^{g}(s) &\approx \frac{1}{2}\left(M_{0h}^{g}(s) - M_{0h}^{g}(\alpha R) + M_{2h}^{g}(s)\right) \\ &= \frac{1}{2}\left(M_{0h}^{g}(s) + M_{2h}^{g}(s)\right) - \frac{1}{2}M_{R,0h}^{g} \end{aligned} \tag{15c}$$

Finally, the complicated equation given in Expression 8 can be replaced with the following, simplified equation:

$$H_{2h}^{g} \approx 2H_{3h}^{g} - H_{0h}^{g} \tag{16}$$

If Equations 6, 8, and 10 are substituted in Equation 16, then the biggest absolute relative difference of -0.4% is obtained for a half-angle of embrace equal to 90°; if the simplified Equation 13 is used instead of Equation 10, the biggest absolute relative difference of -2.2% is obtained when the half-angle of embrace ranges between 72° and 73°;

Equations 14-16 represent another important contribution of this paper, as they establish approximate relationships between the horizontal reactions and between internal forces of the three-hinged, two-hinged and hingeless segmental arches with the same geometrical properties.

3.6. Example of comparative analysis of three-hinged, two-hinged and hingeless segmental arches loaded by self-weight

To understand the theoretical behavior of arches, let's first define normalized internal forces $\tilde{N}$, $\tilde{S}$, and $\tilde{M}$, and normalized eccentricity $\tilde{e}$ as shown in Equations 17. Note that for each cross-section with coordinate *s*, *e*(*s*) represents equivalent eccentricity of normal force in cross-section, i.e., it shows the location of the resultant of stresses in the cross-section (*e*(*s*) practically represents the thrust line).

$$\tilde{N}(s) = \frac{N(s)}{gL};\ \tilde{e}(s) = \frac{e(s)}{L} = \frac{M(s)/N(s)}{L} \tag{17a}$$

$$\tilde{M}(s) = \frac{M(s)}{gL^2} = \tilde{N}(s)\tilde{e}(s) \tag{17b}$$

$$\tilde{S}(s) = \frac{S(s)}{gL} = L\frac{\mathrm{d}\tilde{M}(s)}{\mathrm{d}s} \tag{17c}$$

Normalized diagrams (thrust lines) of hingeless ("0hinge"), two-hinged ("2hinge"), and three-hinged ("3hinge") arches with half-angles of embrace of 21°, 45°, 69°, and 90° are shown in Figure 6. These angles are selected as they represent the upper limit for flat, shallow, moderate, and tall arches (see also Figure 4). To keep the paper concise, diagrams of normalized normal force, bending moment and shear force are not presented; their trends can be inferred from Equations 17b-c.

The diagrams of normalized eccentricity show that for flat arches there is no significant difference in stress distribution between the three structural systems, and the maximum absolute normalized

eccentricities for hingeless, two-hinged, and three-hinged arches is smaller than 0.0005 (for half-angle of embrace of 21°, see Figure 6). This extremely small value (e.g., for 10 m span max. absolute eccentricity is 5 mm) can be explained by the fact that for such a small angle of embrace the difference in shape between circular segment and catenary with the same span and rise is very small, and thus the three types of arches have practically the same behavior as catenary arches under self-weight, i.e., the bending moment is close to zero and consequently eccentricity is close to zero.

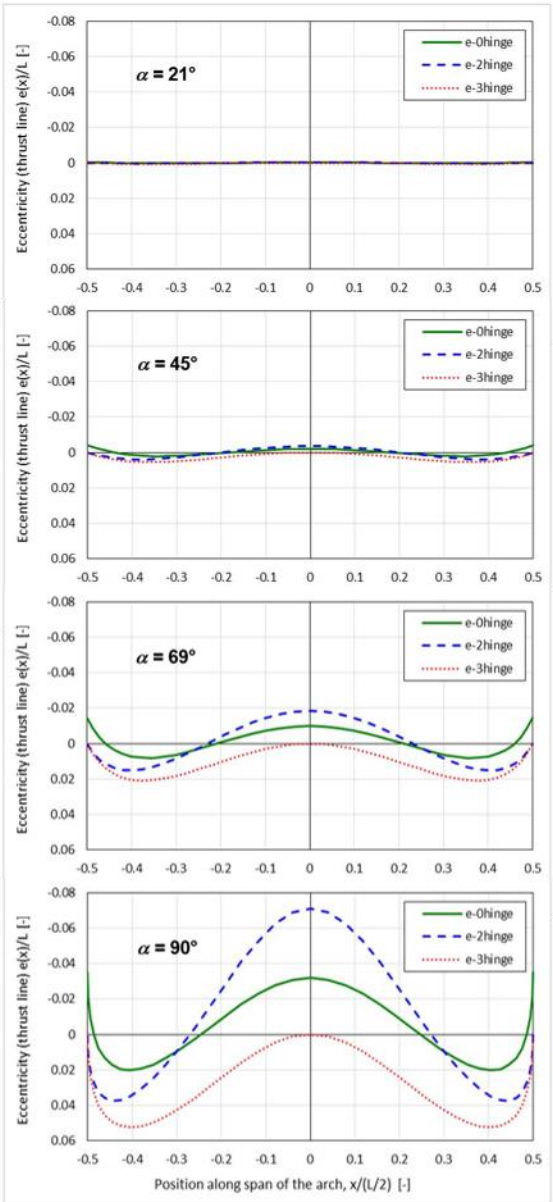

Figure 6: *Normalized diagrams of eccentricity (thrust line) for hingeless (0hinge), two-hinged (2hinge), and three-hinged (3hinge) arches with half-angle of embrace of 21°, 45°, 69°, and 90°; scale is the same for all figures (sign convention: eccentricity is positive below the centroid line)*

For shallow arches, the maximum absolute normalized eccentricity increases with the half-angle of embrace to 0.0042, 0.0039, and 0.0052 for the hingeless, two-hinged, and three-hinged arch, respectively (for 45°, see Figure 6). These values are still very small (e.g., for 10 m span max. absolute eccentricities are 42 mm, 39 mm, and 52 mm) due to similarity in shape to catenary and show that there is a little influence of bending moments and shear forces to stress distribution in all three types of arches, and thus, the three types of arches have very similar behavior, when flat and shallow.

Finally, for arches with moderate rise and tall arches the absolute value of normalized eccentricity further increases with the half-angle of embrace, and reaches 0.0349, 0.0708, and 0.0524 for half-angle of embrace of 90° (see Figure 6). This shows that in tall arches, the hingeless, two-hinged, and three-hinged arch may have significantly different behavior from each other, especially for higher values of half-angles of embrace.

The comparative analysis performed in this subsection is just one of a kind that demonstrates the practicality of the use of closed-form equations to understand structural behavior of arches. Many other studies can be performed, for example focusing on stress analysis, tolerable differential movements of supports, etc.

3.7. Applicability of Equations 13 and 14 to the catenary and parabolic arches

As mentioned in Section 1, it is well known that the ideal shape for an arch loaded with self-weight is the shape of a catenary curve [5]. However, in modern practice, the shape of parabola is frequently used, mostly because it has an ideal shape for the uniformly distributed load along the deck over an arch, its shape is very close to the catenary even for tall arches, and finally, its shape is simple to describe mathematically in Cartesian coordinates (simpler than segment of a circle or catenary), and thus a construction of a parabolic arch is simple. However, closed-form equations for parabolic shape are much more difficult to derive since the radius of geometric curvature R (see Equations 1a-c) is not constant along the arch; in addition, deriving the flexibility coefficients is also very difficult as integration of real and virtual internal forces has to be performed over the parabolic curve using natural (arc-length) parametrization (the parabola has a simple equation in Cartesian coordinates, but very complex when described with natural parametrization).

The applicability of the Equations 13 and 14 (and consequently 15a-c) for catenary and parabolic arches is examined in this section. Figure 7 shows the three arch shapes for four characteristic rise-to-span ratios *D/L*.

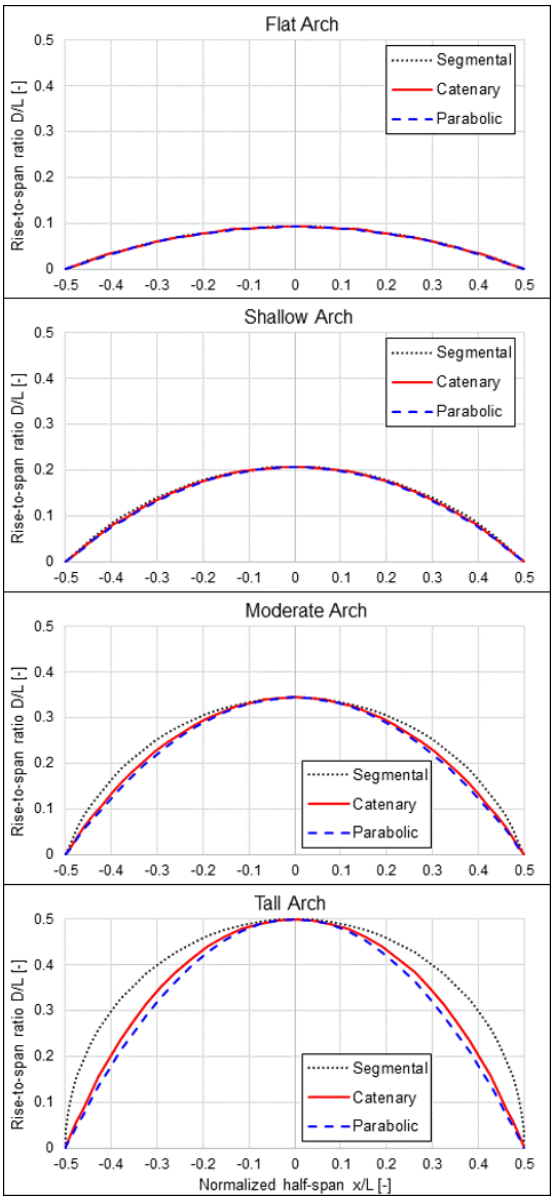

Figure 7: *Comparison of shapes for segmental, catenary, and parabolic arches for typical rise-to-span ratios*

The figure shows that the three curves have almost indistinguishable shapes for flat and shallow arches. The distinction between the shapes becomes visible as the rise-to-span ratio further increases. For moderate and especially for tall arches, the segmental arch has a significant departure from catenary, while parabolic arch has just a mild difference from catenary, showing that for moderate and tall arches the parabolic arch is better suited to carry self-weight than a segmental arch. Table 1 summarizes the normalized horizontal reaction for different shapes of arches and enables evaluation the applicability of simplified Equations 13 and 14 to catenary and parabolic shape.

Table 1: *Normalized horizontal reaction in hingeless segmental, catenary, and parabolic arches for typical rise-to-span ratios*

Arch properties	Rise-to-span ratio (*D/L*)	0.092	0.207	0.344	0.500
	Classification (upper limit)	Flat	Shal-low	Mode-rate	Tall
Normalized horizontal reaction *H/(gL)*	Segmental, hinge-less, (exact, Eq. 10)	1.3684	0.6444	0.4231	0.3197
	Segmental, hinge-less (appr., Eq. 13)	1.3642	0.6366	0.4152	0.3183
	Catenary arch (all types)	1.3641	0.6354	0.4109	0.3094
	Parabolic arch*, hingeless	1.3620	0.6322	0.4088	0.3107
	Parabolic arch*, three-hinged	1.3641	0.636	0.4135	0.3153
	Parabolic arch*, two-hinged	1.3663	0.6409	0.4212	0.3258
Relative difference [%]	Eq. 13 vs. catenary [%]	0.01	0.20	1.04	2.89
	Eq. 13 vs. parabolic hingeless [%]	0.15	0.70	1.55	2.43
	Eq. 13 vs. parabolic three-hinged [%]	0.005	0.09	0.41	0.96
	Eq. 13 vs. parabolic two-hinged [%]	-0.16	-0.66	-1.42	-2.31

*Calculated using numerical integration (four significant figures)

The table shows that the simplified expression given in Equation 13 is applicable to the catenary arch, for all rises, as the relative error in the normalized horizontal reaction is under 3%. The error is practically negligible for flat, shallow and moderate arches as it is under or around 1%. A similar conclusion applies to all three types of parabolic arches, with slightly different figures regarding the accuracy of estimation (see table for details). Table 1 practically shows great versatility in application of Equation 13, as it can be extended to catenary and parabolic arches. However, given that these two forms do not have an angle of embrace, an equivalent angle of embrace can be calculated as shown in Equation 18 and then used in Equation 13 (derivation follows from geometry of arch shown in Figure 1).

$$\beta_{equivalent} = 2\alpha_{equivalent} = 4\arctan\left(2\frac{D}{L}\right) \qquad (18)$$

Note that catenary arch under the self-weight is moment free, which has two consequences: first, the Equation 13 can be applied with the same accuracy

to the three- and two-hinged catenary arches; and second, Equation 14, and consequently Equations 15a-c, are all applicable to three-hinged, two-hinged and hingeless catenary arches.

In addition, Table 1 shows that Equation 14, and consequently Equations 15a-c, are also all applicable to the three-hinged, two-hinged and hingeless parabolic arches under self-weight. There are many other important conclusions that can be carried out from Table 1, e.g., using similar approach as described in Section 3.6. However, further detailed analysis of parabolic arches is out of the scope of this paper.

3.8. Example of extension of work to a different load scenario: uniformly distributed vertical load along arch span

This section briefly presents an example of extension of the work to different load scenario – uniformly distributed vertical load, $q_y(x)=q(x)=q=constant$, along the span of typical segmental arches. This, load corresponds to a self-weight of a deck supported by the arch, as shown in Figure 8. To keep this section concise, only closed equations for reactions are presented in this section along with the most important findings. Also, only hingeless structure is presented in Figure 8 (for three- and two-hinged structure the load is the same).

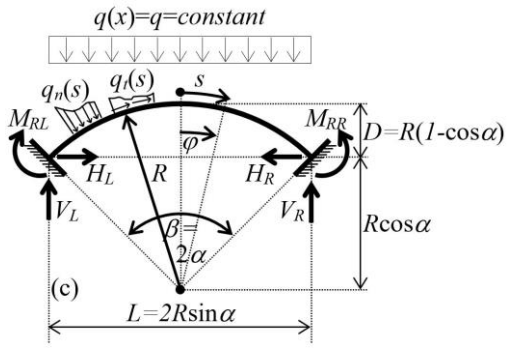

Figure 8: *Uniformly distributed load acting over segmental arch; superscript "q" is omitted in corresponding reactions to simplify presentation*

Vertical reactions in all three types of arches are expressed by Equation 19. Horizontal reactions in three-hinged, two-hinged, and hingeless arch are expressed by Equations 20, 21, and 22, respectively. Moment reaction in hingeless arch is expressed by Equation 23.

Expression for horizontal reaction of three-hinged arch is very simple and intuitive (Equation 20); however, this is not the case for the two other arch types. Equations 21 and 22 cannot be further simplified without loss of accuracy. Thus, the applicability of Equation 20 on two-hinged and hingeless arches is further examined using similar approach as the one taken in Subsection 3.5.

$$V_R^q = V_L^q = V^q = q\frac{L}{2} = qR\sin\alpha \tag{19}$$

$$H_{3h}^q = \frac{1}{8}q\frac{L^2}{D} = qR\cos^2\frac{\alpha}{2} = \frac{1}{4}qL\cot\frac{\alpha}{2} = \frac{qL}{4\tan\frac{\alpha}{2}} \tag{20}$$

$$H_{2h}^q = -\frac{1}{2}qR\cdot \frac{\alpha\cos\alpha\left(\sin^2\alpha-\cos^2\alpha\right)+\sin\alpha\left(1-\frac{7}{3}\sin^2\alpha\right)}{\alpha-3\sin\alpha\cos\alpha+2\alpha\cos^2\alpha}$$

$$= -\frac{1}{4}qL\frac{\alpha\cot\alpha\left(\sin^2\alpha-\cos^2\alpha\right)+\left(1-\frac{7}{3}\sin^2\alpha\right)}{\alpha-3\sin\alpha\cos\alpha+2\alpha\cos^2\alpha} \tag{21}$$

$$H_{0h}^q = -\frac{1}{2}qR\frac{\sin\alpha\left(\frac{2}{3}\sin^2\alpha-1+\frac{\sin\alpha\cos\alpha}{\alpha}\right)}{\alpha+\sin\alpha\cos\alpha-2\frac{\sin^2\alpha}{\alpha}}$$

$$= -\frac{1}{4}qL\frac{\frac{2}{3}\sin^2\alpha-1+\frac{\sin\alpha\cos\alpha}{\alpha}}{\alpha+\sin\alpha\cos\alpha-2\frac{\sin^2\alpha}{\alpha}} \tag{22}$$

$$M_{R,0h}^q = \frac{1}{4}qR^2\left(1-2\sin^2\alpha-\frac{\sin\alpha\cos\alpha}{\alpha}\right.$$

$$\left.-2\frac{\sin\alpha\left(\frac{2}{3}\sin^2\alpha-1+\frac{\sin\alpha\cos\alpha}{\alpha}\right)}{\alpha+\sin\alpha\cos\alpha-2\frac{\sin^2\alpha}{\alpha}}\cdot\left(\frac{\sin\alpha}{\alpha}-\cos\alpha\right)\right) \tag{23}$$

Horizontal reactions of three-hinged and two-hinged arch were normalized with horizontal reaction in hingeless arch and graphed against half-angle of embrace in Figure 9 (compare with Figure 5).

Figure 9 is qualitatively similar to Figure 5, and consequently discussion and conclusions related to Figure 9 are qualitatively the same as those related to Figure 5, presented in bullet points 1-3 in Subsection 3.5. The only practical difference in discussion and conclusions is quantitative. For example, Equation 14 is valid for (can be extended to) load case discussed in this section, i.e., the subscript *g* can be replaced with *q* to obtain:

$$H_{3h}^{q} \approx \frac{1}{2}\left(H_{0h}^{q} + H_{2h}^{q}\right) \tag{24}$$

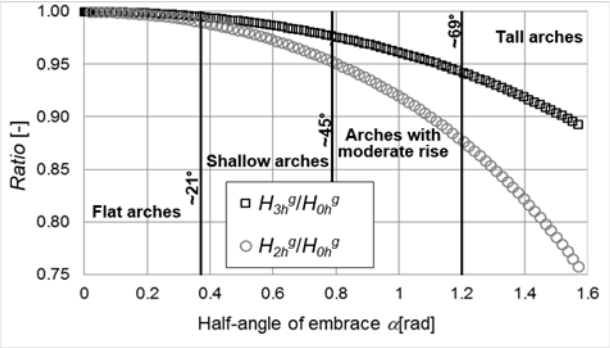

Figure 9: *Ratios between horizontal forces of three-hinged and hingeless arch, and two-hinged and hingeless arch, as functions of half-angle of embrace (uniformly distributed load along the span)*

In Equation 24 the biggest absolute relative difference between the right and left side is -1.6% for half-angle of embrace of 90°, which is higher than for the load case described in Subsection 3.5 (self-weight), but still acceptably small. Therefore, relationships between internal forces of the three-hinged, two-hinged, and hingeless arches follow the same rule as described in Equations 15a-c for self-weight load case.

Given that Equations 21 and 22 cannot be further simplified, it is important to note that, based on Figure 9, the Equation 20 can be extended to two-hinged and hingeless flat and shallow arches, with reasonably good accuracy, to some extent to arches with moderate rise, and even to tall arches, depending on acceptable accuracy. Equation 20 underestimates value of horizontal reaction of hingeless arch as follows: for flat arches less than -0.5%, for shallow arches -0.5% to -2.3%, for arches with moderate rise -2.3% to -5.8%, and for tall arches -5.8% to 10.7%. Equation 21 overestimates value of horizontal reaction of two-hinged arch as follows: for flat arches less than 0.5%, for shallow arches 0.5% to 2.6%, for arches with moderate rise 2.6% to 7.5%, and for tall arches 7.5% to 17.8%.

Given that the load *q* does not depend on arch shape, Equation 20 is valid for any three-hinged arch (regardless the shape) that has the same geometrical location of hinges as the arch shown in Figure 9 (this can be proven from simple equations of equilibrium). Consequently, Equation 20 can be extended to three-hinged parabolic and catenary arches. In addition, parabolic shape is ideal for load *q*, i.e., parabolic arch is moment-free and shear force-free under the load *q*, and therefore, Equation 20 is also applicable to two-hinged and hingeless parabolic arches. Furthermore, given similarity in shape between parabolic and catenary arches (see Figure 7), Equation 20 can also be extended to two-hinged and hingeless catenary arches. The upper limits for maximum absolute error for two-hinged arch are 0.2% for flat, 0.8 for shallow, 1.9% for moderate, and 3.6% for tall arch. The upper limits for maximum absolute error for hingeless arch are -0.2% for flat, -0.6 for shallow, -1.2% for moderate, and -1.7% for tall arch. Hence, Expression 24 (or, extension of Equation 14) also applies to parabolic (exactly) and catenary arches (approximately, with maximum absolute error under -0.9% for equivalent half-angle of embrace of 90°).

Equations given in this section allow for analysis similar to that performed in Subsection 3.6 for self-weight load case, but also for various other types of different analyses. For instance, comparison between the two load cases (self-weight of the arch vs. self-weight of the deck) can be carried out. To illustrate this statement, two examples are given.

In Equation 20, if the values of half-angle of embrace α are small enough, then Equation 25 is valid.

$$\alpha \text{ "small enough"} \Rightarrow$$

$$\tan\frac{\alpha}{2} \approx \frac{\alpha}{2} \Rightarrow H_{3h}^{q} \approx \frac{qL}{2\alpha} = \frac{qL}{\beta} \tag{25}$$

Equation 25 is, practically, an extension of Equation 13 obtained by substitution of *g* with *q*.

For half-angles of embrace α of 21°, 45°, 69° and 90°, Equation 25 underestimates the exact Equation 20 for 1.1%, 5.2%, 12.4% and 21.5%, respectively. Hence, simplified Equation 25 (i.e., Equation 13) can be used instead of the exact Equation 20 in flat and shallow arches with reasonably good accuracy, while for moderate and tall arches the equation gradually loses accuracy. Equation 25 is analogue to Equation 13, and they converge to each other and to exact solutions as the half-angle of embrace approaches to

zero. This is understandable as for very small half-angles of embrace, arch geometry approaches to that of catenary and self-weight approaches to uniformly distributed load along the span of the arch.

As an additional example, Figure 10 compares the moment reactions in hingeless arch exposed to self-weight g (Equation 12) and uniformly distributed load along the span of the arch q (Equation 23), the former is normalized with gL^2 and latter with qL^2.

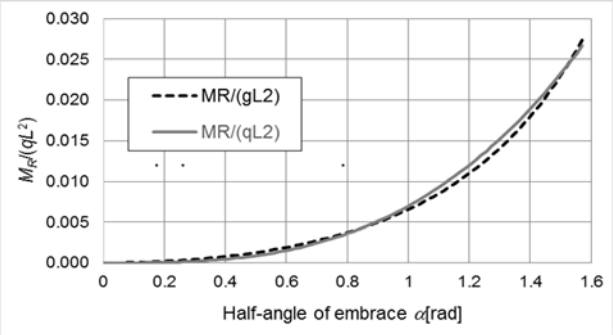

Figure 10: *Normalized moment reactions of hingeless arch loaded by self-weight g and uniformly distributed load q*

Similarity between the two curves is striking, given that for moderate and especially tall arches the distribution of load along the span is significantly different. The maximum relative difference between the two curves is for moderate and tall arches smaller than 8.5%. Closed equations for internal forces can be derived by using Equations 3, and comparative analysis between the three typical structural systems using approach similar to that presented in Subsection 3.6.

4. CONCLUSIONS

Closed-form equations for reactions and internal forces of linear-elastic segmental, catenary, and parabolic arches are explored in this paper, resulting in several important findings and simplifications.

The findings and their interpretations were to a large extent enabled by a simplified formula for determination of the horizontal reactions (thrust) of the hingeless segmental arch under self-weight (Equation 13), which were found to be approximately equal to the product of arch span and linear weight, divided with angle of embrace (expressed in radians). This formula is intuitive, simple to remember and apply, it is valid for all values of angles of embrace between zero (theoretical) and π (180°), and it underestimates the theoretical true value for less than 2% for all rises of the arch (i.e., for all angles of embrace). In addition, the same formula was proven to be also applicable to the catenary and parabolic three-hinged, two-hinged, and hingeless arches with a relative difference within ±3%. Analysis of dependence of normalized horizontal reaction of half-angle of embrace helped classify the arches based on their geometrical properties to flat arches (0°-21°), shallow arches (21°-45°), arches with moderate rise (moderate arches, 45°-69°), and tall arches (69°-90°).

Three important findings related to segmental arches are: the fact that hingeless arch has the highest and the two-hinged arch the lowest magnitude of horizontal reaction (for the same geometrical properties, under self-weight and under uniformly distributed load along the span); the fact that horizontal reaction in three-hinged arch is approximately equal to average value between the horizontal reactions of hingeless and two-hinged arch (Equations 14 and 25); and, as a consequence of the latter, the normal and shear force in the three-hinged arch are approximately equal to the average value between the normal forces and shear forces of hingeless and two-hinged arch (Equations 15a-b). The latter two conclusions apply to parabolic and catenary arches too.

Finally, applicability of closed-form equations was briefly evaluated through comparison of the eccentricity in arches with different geometries, different structural systems, and different loads.

To complete the understanding of linear elastic arches, future research should include the influence of other types of loads and in particular the influence of concentrated force and non-symmetric loads. Also, further comparisons between different structural systems as well as inclusion of one-hinged arch (with hinge at the apex, rarely found in real-life applications), could be included in the future work.

ACKNOWLEDGMENTS

This paper was enthused by the work and the vision of Prof. David P. Billington (1927-2018), Prof. Milutin Milanković (1879-1958), Leonardo da Vinci (1452-1519), Prof. Leopold Pflug, Prof. Nicos Makris, Prof. John Ochsendorf, Prof. Jacques Heyman, Prof. Lynne Lancaster, and my dear colleagues Prof. Sigrid Adriaenssens and Prof. Maria Garlock. Infinite thanks to Dr. Anjali Mehrotra, Ms. Victoria Sassoon, Prof. Tim Michiels, Prof. Isabel Morris, and Prof. Rebecca Napolitano for sparking the ideas on historic arches in Heritage Structures Lab.

REFERENCES

[1] M. Como, *Statics of Historic Masonry Constructions* (2nd Edition), Springer International Publishing Switzerland, 2016. (DOI: 10.1007/978-3-319-24569-0)

[2] C. O'Connor, *Roman Bridges*, Cambridge University Press, 1993.

[3] J. Heyman, *Structural Analysis, A Historical Approach*, Cambridge University Press, 1998. (DOI: 10.1017/CBO9780511529580)

[4] E. MacCurdy, *The Notebooks of Leonardo Da Vinci*, New York: Reynal &Hitchcock, 1939 (Notebooks writing started in 1508).

[5] R. Hooke, "*A description of helioscopes, and some other instruments made by Robert Hooke, Fellow of the Royal Society"*, London: T. R. (for John Martyn Printer to the Royal Society), 1676, (accessed at https://quod.lib.umich.edu/e/eebo/A44317.0001.001?rgn=main;view=fulltext on June 13, 2018).

[6] J.A.C. Bresse, *Recherches analytiques sur la flexion et la résistance des pièces courbées, accompagnées des tables numériques pour calculer la poussée des arcs chargés des poids d'un manière quelconque et leur pression maximum sous une charge uniformément repartie*, Paris: Mallet-Bachelier, 1854.

[7] E. Winkler, "Formänderung und Festigkeit gekrümmter Körper, insbesondere der Ringe," *Civilingenieur*, vol. 4, pp. 232-246, 1858.

[8] C.B. McCullough and E.S. Thayer, *Elastic arch bridges*, New York: John Wiley & Sons, Inc., 1931.

[9] J. Heyman, "The safety of masonry arches," *International Journal of Mechanical Sciences*, vol. 11, pp. 363-385, 1969. (DOI: 10.1016/0020-7403(69)90070-8)

[10] J. Ochsendorf, "The masonry arch on spreading supports," *The Structural Engineer*, vol. 84, pp. 29-34, 2006.

[11] H. Alexakis and N. Makris, "Limit equilibrium analysis of masonry arches," *Archive of Applied Mechanics*, vol. 85, pp. 1363-1381, 2015. (DOI: 10.1007/s00419-014-0963-6)

[12] K-E. Kurrer, *The history of the theory of structures*, Ernst & Sohn (A Wiley Company), 2008.

[13] M. Đurić and O. Đurić-Perić, *Statika Konstrukcija* (4th Edition), Građevinska Knjiga, Belgrade, 1990.

[14] R.C. Hibbeler, *Structural Analysis* (7th Edition), Upper Saddle River (NJ): Prentice Hall, Inc., 2008.

[15] Y.-L. Pi, M.A. Bradford, F. Tin-Loi and R.I. Gilbert, "Geometric and material nonlinear analyses of elastically restrained arches," *Engineering Structures*, vol. 29, pp. 283–295, 2007.(DOI: 10.1016/j.engstruct.2006.01.016)

[16] D. Ait, R. Barsotti and S. Bennati, "Some explicit solutions for nonlinear elastic depressed masonry arches loaded to collapse," *XII Congresso dell'Associazione Italiana di Meccanica Teorica e Applicata Genoa, 14-17 September 2015.*

[17] C.-F. Hua, Y.-L. Pi, W. Gaob and L. Lia, "In-plane non-linear elastic stability of parabolic arches with different rise-to-span ratios," *Thin-Walled Structures*, vol. 129, pp. 74–84, 2018. (DOI: 10.1016/j.tws.2018.03.019)

[18] W.J. Lewis, "Mathematical model of a moment-less arch," *Proceedings of The Royal Society A Mathematical Physical and Engineering Sciences"*, vol. 472, art. no. 20160019, 2016.
(DOI: 10.1098/rspa.2016.0019)

[19] C.Y. Wang and C.M. Wang, "Closed-form solutions for funicular cables and arches," *Acta Mechanica*, vol. 226, pp. 1641–1645, 2015. (DOI: 10.1007/s00707-014-1250-x)

[20] B. Glisic, "Simplified closed-form expressions for horizontal reactions in linear elastic arches under self-weight," *Form and Force, 60th IASS Symposium*, pp. 271-278, 2019.

[21] B. Glisic, "Derivation of closed-form expressions for reactions and internal forces of Linear-Elastic Symmetric segmental arches", *Princeton University*, 2020. https://drive.google.com/file/d/1nY3YrnDDVLWKG_Iil5AwOoYW6bbo0g3t/view?usp=sharing (last accessed on July 7, 2020).